NANO LETTERS

Letter

pubs.acs.org/NanoLett

Electrically Tunable Metasurface Perfect Absorbers for Ultrathin Mid-Infrared Optical Modulators

Yu Yao,[†,#] Raji Shankar,[†] Mikhail A. Kats,[†] Yi Song,[‡] Jing Kong,[‡] Marko Loncar,[†] and Federico Capasso*[,†]

[†]School of Engineering and Applied Sciences, Harvard University, Cambridge, Massachusetts 02138, United States

[‡]Department of Electrical Engineering and Computer Science, Massachusetts Institute of Technology, Cambridge, Massachusetts 02139, United States

Supporting Information

ABSTRACT: Dynamically reconfigurable metasurfaces open up unprecedented opportunities in applications such as high capacity communications, dynamic beam shaping, hyperspectral imaging, and adaptive optics. The realization of high performance metasurface-based devices remains a great challenge due to very limited tuning ranges and modulation depths. Here we show that a widely tunable metasurface composed of optical antennas on graphene can be incorporated into a subwavelength-thick optical cavity to create an electrically tunable perfect absorber. By switching the absorber in and out of the critical coupling condition via the gate voltage applied on graphene, a modulation depth of up to 100% can be achieved. In particular, we demonstrated ultrathin (thickness < $\lambda_0/10$) high speed (up to 20 GHz) optical modulators over a broad wavelength range (5−7 μm). The operating wavelength can be scaled from the near-infrared to the terahertz by simply tailoring the metasurface and cavity dimensions.

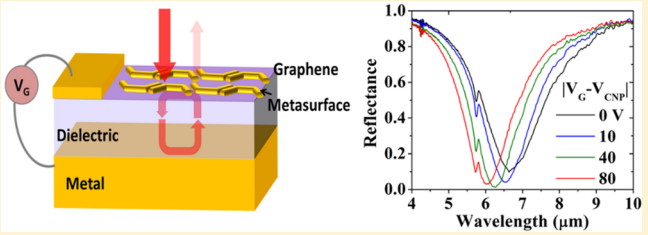

KEYWORDS: *Metasurface perfect absorbers, electrically tunable, graphene, optical modulators, mid-infrared optoelectronics*

Metasurfaces are ultrathin optical components comprising artificially designed arrays of optical scatters, which can impart abrupt changes to the phase and amplitude of incident light over deep-subwavelength length scales.[1,2] Recent progress in metasurfaces has enabled great flexibility in light manipulation[2−4] and led to a variety of flat, ultrathin optical components.[5−10] The development of metasurfaces with reconfigurable optical responses has become a frontier with the promise to achieve reconfigurable flat optics and optoelectronics. There have been great research efforts in developing tuning methods of plasmonic structures based on thermal,[11,12] mechanical,[13] optical,[14] and electrical[15−30] mechanisms. Among these techniques, electrical tuning methods based on graphene[23−29,31] have substantial technological potential in terms of response time, broadband operation, compactness, and compatibility with silicon technology as well as large scale fabrication[32] because graphene has high electrical and thermal conductivity, broadband widely tunable electro-optical properties, and good chemical resistance. However, dynamically tunable metasurfaces have not yet been proved viable for practical applications because the amplitude modulation depth and phase tuning range achieved experimentally so far cannot satisfy the requirements in many applications.

Optical resonators have been used for light modulation, enhanced photodetection, and strong light−matter coupling in various devices.[33−38] Many of these designs are based on the concept of critical coupling,[39−41] which leads to complete light absorption in the resonator, i.e., perfect absorption. In this letter, we demonstrate a high speed tunable metasurface perfect absorber with optical modulation depth up to 100%, by incorporating a widely tunable metasurface on graphene into a subwavelength-thick optical resonator. We also developed an analytical formalism of the perfect absorption condition for rapid structure optimization. On the basis of this idea, we have demonstrated the thinnest (total thickness < $\lambda_0/10$) optical modulators with a maximum modulation depth of more than 95% in the mid-infrared (mid-IR) wavelength range. Furthermore, the tunable metasurface absorbers can be structurally engineered to operate over a broad wavelength range, from near-infrared to terahertz wavelengths, and therefore provide efficient solutions for reconfigurable flat optics and optoelectronics.

Design of the Electrically Tunable Metasurface Perfect Absorber. Our metasurface absorber is composed of a metallic thin film, a dielectric layer and an electrically tunable metasurface comprising plasmonic structures on graphene, as shown in Figure 1a. Similar to metamaterial perfect absorbers,[42,43] the metasurface perfect absorbers can be made much thinner than the operational wavelength. Yet, one major difference between the two is that the former relies on both electric and magnetic response (described as $\varepsilon(\omega)$, $\mu(\omega)$), while the latter does not require magnetic response, which greatly reduces the design and fabrication complexity.

Received: August 12, 2014
Revised: September 29, 2014
Published: October 13, 2014

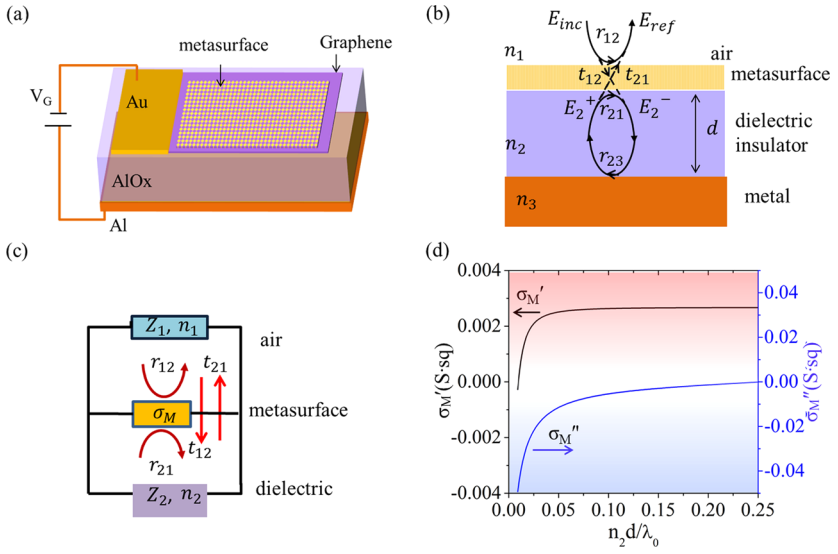

Figure 1. Ultrathin metasurface perfect absorber. (a) Schematic of the tunable metasurface absorber composed of a metasurface on graphene, an aluminum oxide (AlOx) dielectric layer, and an aluminum (Al) substrate. (b) Cross-section view of the metasurface absorber in which we have identified the modified Fresnel coefficient and the complex field amplitudes at each side of the interface. (c) Effective circuit model for reflection and transmission coefficients at the air–dielectric interface with a metasurface of conductivity σ_M. Z_1 and Z_2 are the wave impedance of the air and the dielectric layer, respectively. (d) Calculated real (σ_M') and imaginary (σ_M'') parts of metasurface conductivity required to satisfy the critical coupling condition as a function of the relative dielectric thickness n_2d/λ_0.

This structure can be modeled as an asymmetric Fabry–Perot (FP) resonator with two mirrors, i.e., a tunable metasurface reflector as a partially reflecting mirror in the front and a metallic fully reflecting mirror in the back. Figure 1b illustrates the optical coupling in such a resonator. When a plane wave is incident vertically on the metasurface, the complex amplitudes of the electric field, i.e., E_{inc}, E_{ref}, and E_2^+, E_2^-, at each side of the air-dielectric interface can be written as

$$E_{ref} = r_{12}E_{inc} + t_{21}E_2^+$$
$$E_2^- = t_{12}E_{inc} + r_{21}E_2^+ \quad (1)$$

where the reflection coefficients r_{12} and r_{21} are the ratios of the reflected wave's complex electric field amplitudes to that of the incident waves for light incident on the air-dielectric interface with the metasurface, from the air and from the dielectric substrate, respectively. Likewise the transmission coefficients t_{12} and t_{21} are the ratios of the transmitted wave's complex electric field amplitudes to that of the incident waves for light incident from the air and from the dielectric substrate, respectively. If the reflection coefficient at the metallic back reflector is r_{23} and the thickness of the dielectric layer between the two reflectors is d, then the relationship between the complex amplitudes of the forward wave (E_2^+) and backward wave (E_2^-) beneath the metasurface in the resonator is

$$E_2^+ = E_2^- r_{23}\, e^{i2\beta d} \quad (2)$$

where $\beta = 2\pi n_2/\lambda_0$ is the propagation constant and n_2 is the refractive index of the dielectric layer. Solving eqs 1 and 2, we can obtain the reflection coefficient of the metasurface absorber r_A as

$$r_A = \frac{E_{ref}}{E_{inc}} = \frac{r_{12} + (t_{12}t_{21} - r_{12}r_{21})r_{23}\, e^{i2\beta d}}{1 - r_{21}r_{23}\, e^{i2\beta d}} \quad (3)$$

when $r_A = 0$, all the light is absorbed in the resonator and the critical coupling condition is satisfied. From the relationship between reflection coefficients and transmission coefficients $t_{12} = r_{12} + 1$, $t_{21} = r_{21} + 1$ and setting $r_A = 0$ in eq 3, we can obtain the equation for the critical coupling condition of the metasurface absorber

$$r_{12} + (1 + r_{12} + r_{21})r_{23}\, e^{i2\beta d} = 0 \quad (4)$$

Assume the metasurface optical conductivity is σ_M, the reflection and transmission coefficients for vertically incident light onto the air–dielectric interface can be calculated based on an effective circuit model, as shown in Figure 1c (see Supporting Information I for detailed derivation)

$$r_{12} = \frac{n_1 - n_2 - \sigma_M Z_0}{n_1 + n_2 + \sigma_M Z_0}, \quad r_{21} = \frac{n_2 - n_1 - \sigma_M Z_0}{n_2 + n_1 + \sigma_M Z_0}$$
$$t_{12} = \frac{2n_1}{n_1 + n_2 + \sigma_M Z_0}, \quad t_{12} = \frac{2n_2}{n_1 + n_2 + \sigma_M Z_0} \quad (5)$$

where $Z_0 = (\mu_0/\varepsilon_0)^{1/2}$ is the wave impedance of free space. These equations become the commonly used Fresnel's equations if the metasurface is absent (i.e., $\sigma_M = 0$). We refer to them as modified Fresnel's equations in following discussions. Because of the finite surface conductivity σ_M at the front interface, the typical relationship between the two reflection coefficients $r_{12} + r_{21} = 0$ is not valid. Instead, the two reflection coefficients have different amplitudes as long as $n_1 \neq n_2$. Moreover, even when light is normally incident and the dielectric is lossless, the phase shift of the reflection coefficients can be any value instead of the typical 0 or π as long as σ_M is a complex number. As a result, the critical coupling condition in metasurface resonator cannot be reduced to separate conditions for loss and roundtrip phase, as in most well studied resonators.[40] Furthermore, the roundtrip phase accumulation $2\beta d$ does not have to be close to π, which makes it possible to achieve the critical coupling condition with a much smaller dielectric layer thickness (d) than the wavelength. This is similar to the asymmetric FP resonators formed by ultrathin,

dx.doi.org/10.1021/nl503104n | Nano Lett. 2014, 14, 6526–6532

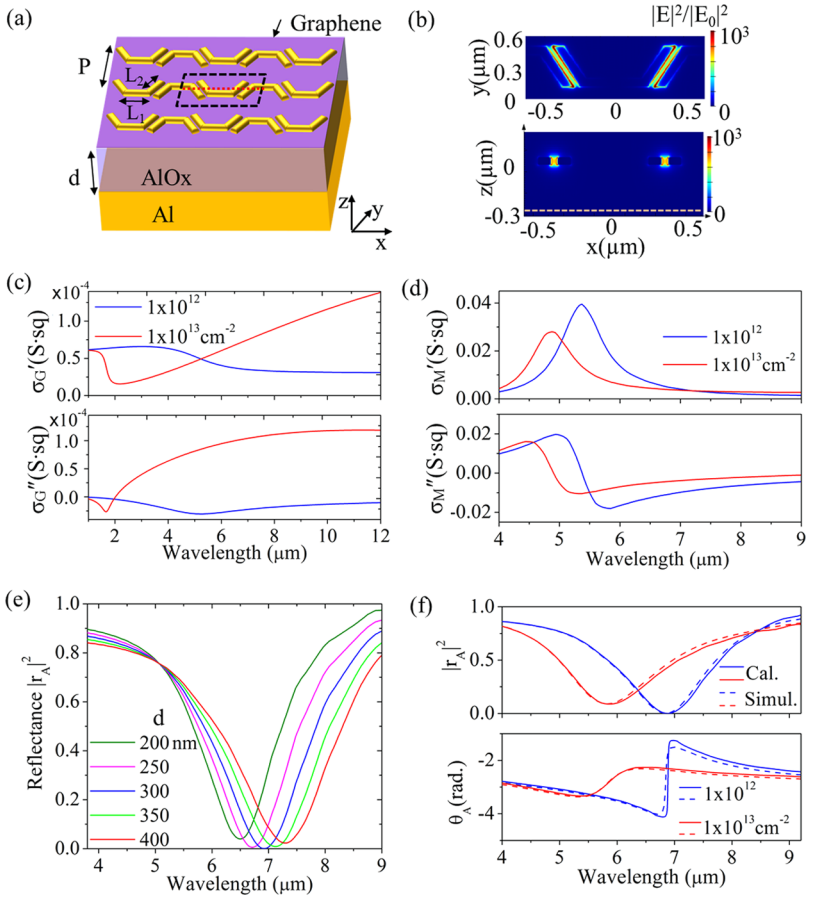

Figure 2. Design of a tunable metasurface perfect absorber. (a) The schematic of a tunable metasurface absorber composed of an aluminum film (thickness 300 nm), aluminum oxide layer (thickness d = 300 nm), and a tunable metasurface on graphene (L_1 = 440 nm, L_2 = 380 nm, P = 600 nm). (b) Full wave simulation results of a unit cell of the metasurface absorber, as indicated by the dashed lines in panel a, when a plane wave is incident vertically onto the surface of the metasurface absorber with electric field polarized along the x-axis. Top: the electric field intensity enhancement distribution $|E|^2/|E_0|^2$ at the horizontal (x–y) plane of the coupled antennas (2 nm above the graphene layer). Bottom: a vertical (x–z) plane cutting through the antennas (indicated with a red dotted line in panel a). (c) Calculated real (σ_G') and imaginary (σ_G'') parts of graphene sheet conductivity for two different charge carrier concentrations, 10^{12} and 10^{13} cm^{-2}. (d) Calculated real (σ_M') and imaginary (σ_M'') parts of metasurface conductivity for two different charge carrier concentrations in the graphene, 10^{12} and 10^{13} cm^{-2}. (e) Calculated reflectance of the metasurface absorbers $|r_A|^2$ with varying dielectric thickness d. (f) The reflectance $|r_A|^2$ and reflection phase shift θ_A of the metasurface absorber for two different charge carrier concentrations. Solid lines: calculation results based on eq 3; dashed lines: simulation results obtained by full wave simulation. The graphene mobility used in all the calculation and simulations is 1000 cm^{-2}/(V s).

absorptive dielectric films;[44−47] however, instead of using highly lossy dielectric layers,[44,45] the present absorber relies on the metasurface, which can be tailored by varying the structure design. Thus, the optical response can be engineered with great flexibility with minimal requirements on the optical constants of the spacer layer. Moreover, the metasurface can be designed with closely coupled antennas, whose optical response is broad tunable via electrostatic doping of graphene.

Inserting eq 5 into eq 4, we can obtain an analytical expression for the surface conductivity of metasurface required for the critical coupling condition (r_A = 0):

$$\sigma_M = \left(n_1 - \frac{n_3 + i n_2 \tan(\beta d)}{1 - i\frac{n_3}{n_2}\tan(\beta d)} \right) \sqrt{\frac{\varepsilon_0}{\mu_0}} \qquad (6)$$

In Figure 1d we plot the real and imaginary parts of the surface conductivity that would result in critical coupling, as obtained by eq 6 for a metasurface absorber (n_1 = 1, n_2 = 1.5, n_3 = 12 + 60i) as a function of the relative dielectric thickness, which is defined as n_2d/λ_0. This plot clearly shows that one can achieve the critical coupling condition in an ultrathin ($n_2d/\lambda_0 \ll 1$) metasurface absorber by engineering the metasurface conductivity. Since the real part of optical conductivity can only be positive under thermal equilibrium (negative optical conductivity means there is optical gain in the material), the thinnest metasurface absorber we can achieve in this configuration is n_2d/λ_0 = 0.01. This analytical solution provides quick and effective guidance in designing metasurface absorbers. For example, when designing an absorber at λ_0 = 7 μm with a 300 nm thick dielectric layer (n_2 = 1.5), i.e., the relative dielectric thickness n_2d/λ_0 is about 0.064, we can obtain the required metasurface conductivity (0.0026 − i0.0089 S·sq) for the critical coupling condition, which can be achieved by tailoring the geometry of the antenna elements comprising the metasurface.

The metasurface used in our design is composed of laterally coupled optical antennas fabricated on a graphene monolayer, which have been previously shown to have widely tunable optical resonances addressable via an applied gate voltage due to the large enhancement of the light−graphene interaction.[27] Figure 2a shows the schematic of the metasurface absorber. The

dx.doi.org/10.1021/nl503104n | Nano Lett. 2014, 14, 6526−6532

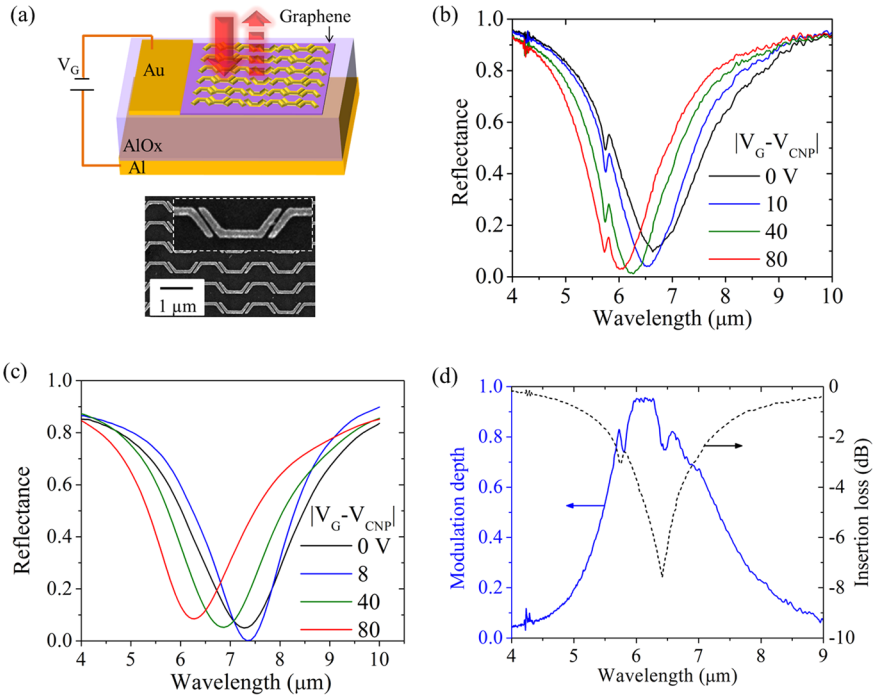

Figure 3. Mid-infrared optical modulator based on an electrically tunable metasurface absorber. (a) Top: schematic of the ultrathin optical modulator based on a tunable metasurface absorber. Bottom: a scanning electron microscope (SEM) image of the metasurface on graphene. Inset: a zoomed-in view of a portion of the metasurface. (b) Simulation results of the reflection spectra from a fabricated metasurface absorbers for different gate voltages. The graphene mobility used in the simulation is obtained by measured transport characteristics (it varies from 200 to 1000 $cm^{-2}/(V\,s)$ depending on the gate voltage, see Supporting Information II). (c) Measured reflection spectra from the metasurface absorber for different gate voltages ($V_G - V_{CNP}$; V_{CNP} is the gate voltage when the concentrations of electrons and holes in the graphene sheet are equal). All spectra are normalized to the reflection spectra from a 300 nm Al film evaporated on the same silicon substrate. (d) The modulation depth achieved experimentally at different wavelength and corresponding insertion loss.

gaps between the coupled antennas are about 40 nm wide, which is much smaller than the wavelength (6–7 μm). When a plane wave is normally incident on the metasurface, the electric field is highly confined in the gap both laterally (in x–y plane) and vertically (along z-axis), as shown in Figure 2b. The highly confined near-field decays over a distance of approximately 50 nm; so as long as the distance between the metasurface and the back-reflector is greater than this value, the effect of the metal reflector on the optical response of the metasurface will be negligible. Thus, we can calculate the reflection and transmission coefficients of the metasurface first using eq 5 and then apply these coefficients in the analytical model of FP resonators (eq 3) to predict the optical response of the metasurface absorber.[48]

The voltage tuning of the metasurface optical response is achieved by electrostatic doping of the graphene sheet underneath the optical antennas. The optical property of graphene is strongly dependent on the charge carrier concentration in the graphene sheet. Figure 2c shows the calculated optical conductivity of graphene based on the random phase approximation (RPA, see detailed information in the Methods section) for two different carrier concentrations. Yet, both the real and imaginary parts of graphene sheet conductivity are on the order of 10^{-5}–10^{-4} S·sq, which is about 2 orders of magnitude smaller than the required metasurface conductivity for the critical coupling condition. As a comparison, the optical conductivity of the metasurface on graphene is much larger and also very sensitive to the carrier concentration of the graphene because of the highly enhanced light graphene interaction in the antenna nanogaps,[27] as shown in Figure 2d. Therefore, we used metasurface on graphene instead of pure graphene and designed a metasurface absorber to achieve close-to-unity absorption at $\lambda_0 = 7$ μm. A parameter scan of dielectric thickness d is performed, and the reflectance ($|r_A|^2$) of metasurface absorbers with the same metasurface and graphene charge carrier concentration (10^{12} cm^{-2}) but different dielectric layer thickness is shown in Figure 2e. An optimized dielectric thickness of 300 nm is obtained for the minimized reflection at the dip.

Using eq 5, we calculate the reflection coefficients of the metasurface absorber for two different carrier concentrations in the graphene layer and then use eq 3 to obtain the reflectance ($|r_A|^2$) as well as the phase shift (θ_A) of the reflected wave, as shown in Figure 2f. At the lower charge carrier concentration, i.e., 10^{12} cm^{-2}, the critical coupling condition is satisfied around 6.9 μm, where the reflectance is approximately zero. When the carrier concentration increases to 10^{13} cm^{-2}, the metasurface conductivity changes (Figure 2d) and the critical coupling condition can no longer be satisfied. The wavelength at which the reflectance minimum occurs is blue-shifted and the reflectance reaches a minimum value of 0.1, which agrees well with the full wave simulation results (see more details about the simulation in the Methods section), as also given in Figure 2f. With such a structure, an optical modulation depth close to 100% can be achieved at wavelengths around 6.9 μm for the reflected light.

Experiments. The metasurface absorber is fabricated on a silicon substrate. The fabrication starts with evaporation of 300 nm aluminum layer onto the top surface of the silicon wafer, followed by atomic layer deposition (ALD) of 300 nm of

dx.doi.org/10.1021/nl503104n | Nano Lett. 2014, 14, 6526–6532

aluminum oxide (AlOx). Then a monolayer graphene sheet (grown via chemical vapor deposition (CVD)) was transferred onto the AlOx layer. The antenna array was fabricated on the graphene sheet by electron beam lithography (EBL), electron beam evaporation of 10 nm Pd and 30 nm Au, and lift-off. Figure 3a shows a schematic of a fabricated device and a scanning electron microscope (SEM) image of the metasurface on graphene.

The reflectance of our devices was measured using a Fourier transform infrared (FTIR) spectrometer with a mid-IR microscope. Light from the FTIR is focused on the device with a mid-IR microscope objective (NA = 0.4), and the reflected light is collected and measured with a mercury cadmium telluride (MCT) detector (see more details in the Methods section). The reflection spectra were collected at different gate voltages applied to the graphene. Figure 3b,c shows the simulated and measured reflectance from the same device, which agree well with each other. From the electrical transport characterization of our graphene sample, we can determine the charge neutral point V_{CNP} = 0 V (where the concentrations of electrons and holes are the same in the graphene) and the carrier mobility, which is used in the full wave simulation to obtain the simulated reflectance (see more details in Supporting Information II). As the gate voltage is tuned away from the charge neutral point the charge carrier concentration in the graphene sheet increases and the metasurface resonance is blue-shifted, as shown in Figure 2d, thus leading to blue shift of the reflectance minimum, as can be inferred from Figure 1d. When the gate voltage $|V_G - V_{CNP}|$ increases to 40 V, the measured reflectance minimum decreases to its lowest value at wavelength around 6.3 μm, then it starts to increase as the gate voltage is further increased. Note that the small feature around 5.77 μm in the measurement results corresponds to the absorption of residual ebeam resist (see more details in Supporting Information III).

Such a metasurface absorber can be used as an optical modulator in reflection mode. As the gate voltage is swept from 0 to 80 V, a wide range of reflectance values can be achieved for each wavelength. The maximum achievable modulation depth for a particular wavelength λ, (i.e., $1 - |((r_{A,min}(\lambda))/(r_{A,max}(\lambda)))|^2$ where $|r_{A,max}(\lambda)|^2$ and $|r_{A,min}(\lambda)|^2$ are the maximum and minimum achievable reflectivity for that wavelength, respectively), is calculated based on the experimental results and plotted as a function of wavelength in Figure 3d. We conclude that our device achieves a modulation depth of more than 95% at 6 μm and more than 50% over a broad wavelength range of 5.4 to 7.3 μm. The modulation depth can be further increased by optimizing the structure and minimizing the reflectance minimum around the critical coupling condition. Another important factor for a modulator is the insertion loss, which is the optical loss when the light intensity is maximized, i.e., $10\log(|r_{A,max}(\lambda)|^2)$ in unit of dB, also shown in Figure 3d. The current range for insertion loss is between −2 to −8 dB, which can be decreased by improving the wavelength tuning range of the reflection dip.

Because if the high conductivity and short optical response time of graphene,[49,50] our tunable absorber can be used as a very fast modulator. We experimentally verified that the response time of our device is shorter than 10 ns, which is limited by the response time of the mid-infrared mercury cadmium telluride (MCT) detector used in our experiment. On the basis of a successful small-signal high-frequency circuit model,[27] we estimate that our modulator (area: 900 μm^2) has a 3 dB cutoff frequency of 20 GHz (see Methods and Supporting Information IV for details of the measurement and modulation speed analysis).

Conclusions. We have demonstrated electrically tunable metasurface absorbers with strong light modulation effect by incorporating a metasurface on graphene into an asymmetric Fabry−Perot resonator, which has a total thickness less than $\lambda_0/10$. In particular, optical modulators have been achieved with a maximum modulation depth over 95% and modulation speed up to tens of GHz over a spectral range in the mid-infrared wavelength. The high speed tunable metasurface absorber design can be scaled from the near-infrared to the terahertz frequency ranges, thanks to the great flexibility in tailoring the response of metasurfaces combined with the broadband optical response of graphene. Therefore, this technology can be used in flat optics and optoelectronics for high capacity communications, hyperspectral imaging, and spatial light modulation and optical switching.

Methods. *Modeling and Simulation.* In the FDTD simulations (Lumerical Solutions, Inc., http://www.lumerical.com/), the graphene layer is modeled as an anisotropic material with in-plane permittivity $\varepsilon_{\parallel}$ and out of plane permittivity $\varepsilon_{\perp}$. The former is calculated from the graphene sheet optical conductivity and the latter is assumed to be 2.5.[51]

The graphene sheet optical conductivity is derived within the random-phase approximation (RPA) in the local limit.[26,52,53]

$$\sigma_s(\omega) = \frac{i2e^2k_BT}{\pi\hbar^2(\omega + i\tau^{-1})}\ln\left[2\cosh\left(\frac{E_F}{2k_BT}\right)\right] + \frac{e^2}{4\hbar}\left[\frac{1}{2} + \frac{1}{\pi}\arctan\left(\frac{\hbar\omega - 2E_F}{2k_BT}\right) - \frac{i}{2\pi}\ln\frac{(\hbar\omega + 2E_F)^2}{(\hbar\omega - 2E_F)^2 + 4(k_BT)^2}\right]$$

where k_B is the Boltzmann constant, T is the temperature, ω is the frequency, τ is the carrier relaxation lifetime, and E_F is the Fermi level. The carrier relaxation time τ can be derived by the measured conductivity and corresponding graphene Fermi level[26]

$$\tau = \sigma\frac{h}{g_s g_v e^2}\frac{2\hbar}{E_F}$$

Reflection Spectra Measurements. Spectral measurements were taken from an 80 μm × 80 μm aperture in a MIR microscope (Bruker Hyperion 2000). The frequency resolution is 2 cm^{-1}, and every spectrum is averaged over 100 scans.

Optical Modulation Measurements. In the optical modulation speed measurement, we apply a sine wave output voltage (offset 0 V, amplitude 5 V) from a function generator (Agilent 33220A) to the back gate of a sample. The output of a single mode continuous wave quantum cascade laser with emission wavelength ~4.5 μm is focused onto our structure using a MIR objective (NA = 0.2) with the incident polarization along the x-axis (the same as that depicted in Figure 2b). The reflected light is collected by the objective. After a beam splitter (45/55), the reflected light is focused onto a thermoelectrically cooled mercury cadmium telluride (MCT) detector (response time < 10 ns). The output of the detector is measured with an oscilloscope to determine the modulation depth.

dx.doi.org/10.1021/nl503104n | Nano Lett. 2014, 14, 6526−6532

■ ASSOCIATED CONTENT

Supporting Information

Derivation of modified Fresnel's equations, electrical transport characterization of the graphene samples, absorption spectra of ebeam resist PMMA, and measurement and calculation of modulation speed. This material is available free of charge via the Internet at http://pubs.acs.org.

■ AUTHOR INFORMATION

Corresponding Author

*E-mail: capasso@seas.harvard.edu. Phone: 1-617-384-7611. Pierce 205A, 29 Oxford Street, Cambridge, MA 02138.

Present Address

#Pierce 205A, 29 Oxford Street, Cambridge, MA 02138

Notes

The authors declare no competing financial interest.

■ ACKNOWLEDGMENTS

We gratefully acknowledge discussions with F. Aieta and P. Genevet. Device fabrication was performed at the Center for Nanoscale Systems, which is a member of the National Nanotechnology Infrastructure Network supported by the National Science Foundation (NSF). This research is supported in part by the Air Force Office of Scientific Research under grant number FA9550-12-1-0289 and by IARPA under grant N66001-13-1-2007 vice N66001-13-1-3005. M.L. and R.S. gratefully acknowledge the financial support by NSF via the collaborative research grant EECS-1028519.

■ REFERENCES

(1) Yu, N. F.; Capasso, F. *Nat. Mater.* **2014**, *13*, 139−150.
(2) Holloway, C. L.; Kuester, E. F.; Gordon, J. A.; O'Hara, J.; Booth, J.; Smith, D. R. *IEEE Trans. Antennas Propag.* **2012**, *54*, 10−35.
(3) Yu, N. F.; Genevet, P.; Kats, M. A.; Aieta, F.; Tetienne, J. P.; Capasso, F.; Gaburro, Z. *Science* **2011**, *334*, 333−337.
(4) Aieta, F.; Genevet, P.; Yu, N. F.; Kats, M. A.; Gaburro, Z.; Capasso, F. *Nano Lett.* **2012**, *12*, 1702−1706.
(5) Aieta, F.; Genevet, P.; Kats, M. A.; Yu, N. F.; Blanchard, R.; Gahurro, Z.; Capasso, F. *Nano Lett.* **2012**, *12*, 4932−4936.
(6) Yu, N. F.; Aieta, F.; Genevet, P.; Kats, M. A.; Gaburro, Z.; Capasso, F. *Nano Lett.* **2012**, *12*, 6328−6333.
(7) Genevet, P.; Yu, N. F.; Aieta, F.; Lin, J.; Kats, M. A.; Blanchard, R.; Scully, M. O.; Gaburro, Z.; Capasso, F. *Appl. Phys. Lett.* **2012**, *100*, 013101.
(8) Spinelli, P.; Verschuuren, M. A.; Polman, A. *Nat. Commun.* **2012**, *3*, 692.
(9) Kildishev, A. V.; Boltasseva, A.; Shalaev, V. M. *Science* **2013**, *339*, 6125.
(10) Lin, D.; Fan, P.; Hasman, E.; Brongersma, M. L. *Science* **2014**, *345*, 298−302.
(11) Xu, G.; Huang, C. M.; Tazawa, M.; Jin, P.; Chen, D. M. *J. Appl. Phys.* **2008**, *104*, 053102.
(12) Kats, M. A.; Blanchard, R.; Genevet, P.; Yang, Z.; Qazilbash, M. M.; Basov, D. N.; Ramanathan, S.; Capasso, F. *Opt. Lett.* **2013**, *38*, 368−370.
(13) Huang, F. M.; Baumberg, J. J. *Nano Lett.* **2010**, *10*, 1787−1792.
(14) Abb, M.; Albella, P.; Aizpurua, J.; Muskens, O. L. *Nano Lett.* **2011**, *11*, 2457−2463.
(15) Kossyrev, P. A.; Yin, A. J.; Cloutier, S. G.; Cardimona, D. A.; Huang, D. H.; Alsing, P. M.; Xu, J. M. *Nano Lett.* **2005**, *5*, 1978−1981.
(16) Berthelot, J.; Bouhelier, A.; Huang, C. J.; Margueritat, J.; Colas-des-Francs, G.; Finot, E.; Weeber, J. C.; Dereux, A.; Kostcheev, S.; El Ahrach, H. I.; Baudrion, A. L.; Plain, J.; Bachelot, R.; Royer, P.; Wiederrecht, G. P. *Nano Lett.* **2009**, *9*, 3914−3921.
(17) Driscoll, T.; Kim, H. T.; Chae, B. G.; Kim, B. J.; Lee, Y. W.; Jokerst, N. M.; Palit, S.; Smith, D. R.; Di Ventra, M.; Basov, D. N. *Science* **2009**, *325*, 1518−1521.
(18) Samson, Z. L.; MacDonald, K. F.; De Angelis, F.; Gholipour, B.; Knight, K.; Huang, C. C.; Di Fabrizio, E.; Hewak, D. W.; Zheludev, N. I. *Appl. Phys. Lett.* **2010**, *96*, 143105.
(19) Chen, H. T.; Padilla, W. J.; Zide, J. M. O.; Gossard, A. C.; Taylor, A. J.; Averitt, R. D. *Nature* **2006**, *444*, 597−600.
(20) Chan, W. L.; Chen, H. T.; Taylor, A. J.; Brener, I.; Cich, M. J.; Mittleman, D. M. *Appl. Phys. Lett.* **2009**, *94*, 213511.
(21) Zhao, Q.; Kang, L.; Du, B.; Li, B.; Zhou, J.; Tang, H.; Liang, X.; Zhang, B. Z. *Appl. Phys. Lett.* **2007**, *90*, 011112.
(22) Buchnev, O.; Ou, J. Y.; Kaczmarek, M.; Zheludev, N. I.; Fedotov, V. A. *Opt. Express* **2013**, *21*, 1633−1638.
(23) Kim, J.; Son, H.; Cho, D. J.; Geng, B. S.; Regan, W.; Shi, S. F.; Kim, K.; Zettl, A.; Shen, Y. R.; Wang, F. *Nano Lett.* **2012**, *12*, 5598−5602.
(24) Emani, N. K.; Chung, T. F.; Ni, X. J.; Kildishev, A. V.; Chen, Y. P.; Boltasseva, A. *Nano Lett.* **2012**, *12*, 5202−5206.
(25) Lee, S. H.; Choi, M.; Kim, T. T.; Lee, S.; Liu, M.; Yin, X.; Choi, H. K.; Lee, S. S.; Choi, C. G.; Choi, S. Y.; Zhang, X.; Min, B. *Nat. Mater.* **2012**, *11*, 936−941.
(26) Yao, Y.; Kats, M. A.; Genevet, P.; Yu, N. F.; Song, Y.; Kong, J.; Capasso, F. *Nano Lett.* **2013**, *13*, 1257−1264.
(27) Yao, Y.; Kats, M. A.; Shankar, R.; Song, Y.; Kong, J.; Loncar, M.; Capasso, F. *Nano Lett.* **2014**, *14*, 214−219.
(28) Emani, N. K.; Chung, T. F.; Kildishev, A. V.; Shalaev, V. M.; Chen, Y. P.; Boltasseva, A. *Nano Lett.* **2014**, *14*, 78−82.
(29) Mousavi, S. H.; Kholmanov, I.; Alici, K. B.; Purtseladze, D.; Arju, N.; Tatar, K.; Fozdar, D. Y.; Suk, J. W.; Hao, Y. F.; Khanikaev, A. B.; Ruoff, R. S.; Shvets, G. *Nano Lett.* **2013**, *13*, 1111−1117.
(30) Fang, Z. Y.; Thongrattanasiri, S.; Schlather, A.; Liu, Z.; Ma, L. L.; Wang, Y. M.; Ajayan, P. M.; Nordlander, P.; Halas, N. J.; de Abajo, F. J. G. *ACS Nano* **2013**, *7*, 2388−2395.
(31) Dabidian, N.; Kholmanov, I.; Tatar, A. B. K. K.; Trendafilov, S.; Mousavi, S. H.; Magnuson, C.; Ruoff, R. S.; Shvets, G. *arXiv:1405.0991* **2014**.
(32) Bae, S.; Kim, H.; Lee, Y.; Xu, X. F.; Park, J. S.; Zheng, Y.; Balakrishnan, J.; Lei, T.; Kim, H. R.; Song, Y. I.; Kim, Y. J.; Kim, K. S.; Ozyilmaz, B.; Ahn, J. H.; Hong, B. H.; Iijima, S. *Nat. Nanotechnol* **2010**, *5*, 574−578.
(33) Yan, R. H.; Simes, R. J.; Coldren, L. A. *IEEE J. Quantum Electron.* **1991**, *27*, 1922−1931.
(34) Yan, R. H.; Simes, R. J.; Coldren, L. A. *IEEE Photonics Technol. Lett.* **1989**, *1*, 273−275.
(35) Prank, U.; Mikulla, M.; Kowalsky, W. *Appl. Phys. Lett.* **1993**, *62*, 129−130.
(36) Furchi, M.; Urich, A.; Pospischil, A.; Lilley, G.; Unterrainer, K.; Detz, H.; Klang, P.; Andrews, A. M.; Schrenk, W.; Strasser, G.; Mueller, T. *Nano Lett.* **2012**, *12*, 2773−2777.
(37) Kishino, K.; Unlu, M. S.; Chyi, J. I.; Reed, J.; Arsenault, L.; Morkoc, H. *IEEE J. Quantum Electron.* **1991**, *27*, 2025−2034.
(38) Tischler, J. R.; Bradley, M. S.; Bulovic, V. *Opt. Lett.* **2006**, *31*, 2045−2047.
(39) Haus, H. A. *Waves and Fields in Optoelectronics*; Prentice-Hall: Englewood Cliffs, NJ, 1984; p xii.
(40) Yariv, A. *IEEE Photonics Technol. Lett.* **2002**, *14*, 483−485.
(41) Thongrattanasiri, S.; Koppens, F. H.; Garcia de Abajo, F. J. *Phys. Rev. Lett.* **2012**, *108*, 047401.
(42) Landy, N. I.; Sajuyigbe, S.; Mock, J. J.; Smith, D. R.; Padilla, W. J. *Phys. Rev. Lett.* **2008**, *100*, 207402.
(43) Watts, C. M.; Liu, X. L.; Padilla, W. J. *Adv. Mater.* **2012**, *24*, Op98−Op120.
(44) Kats, M. A.; Blanchard, R.; Genevet, P.; Capasso, F. *Nat. Mater.* **2013**, *12*, 20−24.
(45) Kats, M. A.; Sharma, D.; Lin, J.; Genevet, P.; Blanchard, R.; Yang, Z.; Qazilbash, M. M.; Basov, D. N.; Ramanathan, S.; Capasso, F. *Appl. Phys. Lett.* **2012**, *101*, 221101.

(46) Kats, M. A.; Blanchard, R.; Ramanathan, S.; Capasso, F. *Opt. Photonics News* **2014**, *25*, 44−47.
(47) Dotan, H.; Kfir, O.; Sharlin, E.; Blank, O.; Gross, M.; Dumchin, I.; Ankonina, G.; Rothschild, A. *Nat. Mater.* **2013**, *12*, 158−164.
(48) Chen, H. T. *Opt. Express* **2012**, *20*, 7165−7172.
(49) George, P. A.; Strait, J.; Dawlaty, J.; Shivaraman, S.; Chandrashekhar, M.; Rana, F.; Spencer, M. G. *Nano Lett.* **2008**, *8*, 4248−4251.
(50) Dawlaty, J. M.; Shivaraman, S.; Chandrashekhar, M.; Rana, F.; Spencer, M. G. *Appl. Phys. Lett.* **2008**, *92*, 042116.
(51) Falkovsky, L. A. *J. Phys.: Conf. Ser.* **2008**, *129*, 012004.
(52) Falkovsky, L. A.; Pershoguba, S. S. *Phys. Rev. B* **2007**, *76*, 153410.
(53) Falkovsky, L. A.; Varlamov, A. A. *Eur. Phys. J. B* **2007**, *56*, 281−284.

dx.doi.org/10.1021/nl503104n | *Nano Lett.* 2014, 14, 6526−6532